Maximal Abelian and Curci-Ferrari gauges in momentum subtraction at three loops

J. M. Bell and J. A. Gracey

Theoretical Physics Division, Department of Mathematical Sciences, University of Liverpool,
P.O. Box 147, Liverpool L69 3BX, United Kingdom
(Received 10 December 2014; published 1 December 2015)

The vertex structure of QCD fixed in the maximal Abelian gauge (MAG) and Curci-Ferrari gauge is analyzed at two loops at the fully symmetric point for the 3-point functions corresponding to the three momentum subtraction (MOM) renormalization schemes. Consequently, the three-loop renormalization group functions are determined for each of these three schemes in each gauge using properties of the renormalization group equation.

I. INTRODUCTION

Four-dimensional gauge theories are of interest due to their description of the elementary quanta of nature. For instance, quantum chromodynamics (QCD) underpins our theoretical understanding of the strong nuclear force where the basic fields are quarks and gluons. These behave as effectively free particles but only in the high-energy limit due to asymptotic freedom, [1,2]. At low energies quarks and gluons are actually confined and do not exist in nature as free particles. The reason why this is the case is one of the major problems in quantum field theory. Various ideas as to the specific confinement mechanism have been proposed. One which is popular is the dual superconductor ideas of [3–6]. There the color electric flux is restricted by the Meissner effect of superconductivity. The role of the Cooper pair condensation of superconductivity is played by the condensation of color magnetic monopoles in the non-Abelian gauge theory case. While this picture parallels superconductivity, it is difficult to access the underlying dynamics practically. One approach is to use an Abelian projection [3,4,6,7] which appears to give insight into low-energy properties of color confinement. For a non-Abelian gauge theory the maximal Abelian sector derives from the centralizer of the color group. Clearly, as such phenomena lie deep within the infrared nonperturbative regime, they can only theoretically be examined by lattice regularized gauge theory or Schwinger-Dyson techniques. Underlying both approaches is the need to isolate the Abelian degrees of freedom to effect a study of this monopole model. Linked to this in a Lagrangian analysis is the need to fix the gauge. Ordinarily one computes in linear covariant gauges such as the Landau gauge. However, this does not have the feature of readily distinguishing the color group centralizer which is related to the Abelian projection. A more appropriate gauge is the maximal Abelian gauge (MAG) introduced in [6,8,9]. There the gluons in the sectors delineated by whether their associated generators totally commute among themselves or not are gauge fixed

differently. For instance, the diagonal gluons, corresponding to the subgroup of generators which totally commute, are fixed in the Landau gauge but the remaining off-diagonal gluons are gauge fixed by a different fixing criterion [6,8,9]. Ultimately, a covariant but nonlinear gauge fixing emerges but in a way which produces a renormalizable Lagrangian. The renormalizability has been established in [10–15]. Properties of the MAG have been studied in various contexts. An interesting recent lattice study, for instance, was in [16] where the effect of the diagonal gluons on the interquark static potential was examined. In particular within the theoretical setup it was possible to identify the contributions made by the diagonal gluons to the potential. Excluding these it was demonstrated [16] that the linearly rising potential collapsed indicating that the Abelian sector was effectively responsible for quark confinement.

As such infrared lattice studies are important, from a more theoretical point of view the Lagrangian field theory focus is concerned with the 2- and 3-point functions of QCD. The low-energy behavior of the former Green's function diverges from the canonical structure of a fundamental particle [17–27], while the latter are studied to assist with building models of hadrons for instance. Therefore Schwinger-Dyson studies have centered on the properties of these Green's functions and particularly in the MAG [28–30]. Lattice studies in the MAG can be found, for instance, in [31–36]. Related to this is the need to ultimately overlap with conventional perturbative analyses. Lattice measurements of vertex functions and Schwinger-Dyson studies have to consistently match onto known perturbation theory. This was partly the motivation to a previous study, [37], where the structure of the 3-point vertices of the MAG fixed QCD Lagrangian were evaluated at one loop at the completely symmetric point. One reason for examining these functions at this point is that this momentum configuration is nonexceptional. So there are no infrared issues unlike the case where the external momentum of one external leg is nullified. Although the

latter is a much more widely studied configuration. As a corollary of the one-loop analysis of [37] the momentum subtraction (MOM) scheme renormalization group functions of the MAG were derived at two loops from properties of the renormalization group equation. In this context as well as the need for previous matching of vertex functions for lattice and Schwinger-Dyson techniques it is the purpose of this article to extend the results of [37] to the next loop order. By this we mean the full structure of the two-loop vertex functions corresponding to the MOM schemes, introduced by Celmaster and Gonsalves in [38,39], and hence deduce the three-loop renormalization group functions. A separate but parallel motivation concerns the relation of the MAG to another nonlinear covariant gauge fixing. This is the Curci-Ferrari gauge which involves a quartic ghost interaction unlike the canonical linear covariant gauge. This gauge fixing was introduced in [40] in part to study massive vector bosons without symmetry breaking. A mass term for the gluons and ghosts could be introduced in a Becchi-Rouet-Stora-Tyutin (BRST) invariant way. In relation to the MAG the Curci-Ferrari gauge fixed Lagrangian emerges in a specific limit. This is the case when the diagonal fields are formally removed from the MAG Lagrangian. Aside from the diagonal gluons this includes the associated diagonal ghosts which together with the off-diagonal ghosts derive from the Faddeev-Popov technique, [8–15]. Therefore, the emerging MOM renormalization group functions in the same limit must agree precisely with those of the Curci-Ferrari gauge. These are also computed directly here as an important independent check on the MAG results. One interesting feature of the MAG, which may have bearing on the infrared properties alluded to already, is that the diagonal gluons appear to play a similar role to the background gluons of the background field gauge of [41–46]. This is because the anomalous dimension of the diagonal gluon is precisely proportional to the β function. This has been established to all orders in perturbation theory from the Slavnov-Taylor identities constructed during the algebraic renormalization proof of the renormalizability of the MAG, [15].

The paper is organized as follows. In the two subsequent sections we introduce and review all the relevant renormalization background and computation methods required for our study of MAG and Curci-Ferrari gauges in QCD at the fully symmetric point of the 3-point vertices. The results of the application of this formalism are given in Sec. IV. Finally, conclusions are presented in Sec. V.

II. BACKGROUND

In this section we record the relevant aspects of the MAG and its relation to the Curci-Ferrari gauge for renormalization at the symmetric point in the various MOM renormalization schemes of [38,39] including the structure of the gauge fixed QCD Lagrangian in the MAG. The main ingredient for the MAG is that the diagonal gluons are treated differently from the off-diagonal ones. Therefore, in keeping with other work, [15], we write the group valued gluon field $\mathcal{A}_\mu$ as

$$\mathcal{A}_\mu \equiv A_\mu^A T^A = A_\mu^a T^a + A_\mu^i T^i, \qquad (2.1)$$

where T^A are the color group generators. On notation we will use upper case roman letters, such as A, B, C and D, for adjoint color indices but lower case where the associated field is either in the center or is off-diagonal. These are distinguished by using a, b, c and so on for the off-diagonal fields except that i, j, k and l are reserved exclusively and unambiguously for diagonal indices. Therefore, each set of indices run over different ranges which are $1 \leq A \leq N_A$, $1 \leq a \leq N_A^o$, and $1 \leq i \leq N_A^d$. (We use the notation of [47] throughout.) Here N_A is the dimension of the adjoint representation of the color group, N_A^d is the dimension of the diagonal subgroup with N_A^o being the dimension of the off-diagonal sector. Clearly,

$$N_A^d + N_A^o = N_A. \qquad (2.2)$$

For reference, if the color group is $SU(N_c)$ then $N_A^d = (N_c - 1)$ and $N_A^o = N_c(N_c - 1)$. With this splitting of the gluons into separate sectors one has to reconsider the canonical group theory required to perform the loop computations. The necessary relations can be established from the usual group identities such as the definition of the group Casimirs and Jacobi identities. For instance,

$$\mathrm{Tr}(T^a T^b) = T_F \delta^{ab}, \qquad \mathrm{Tr}(T^a T^i) = 0,$$
$$\mathrm{Tr}(T^i T^j) = T_F \delta^{ij} \qquad (2.3)$$

follow from

$$\mathrm{Tr}(T^A T^B) = T_F \delta^{AB}. \qquad (2.4)$$

Equally, by allowing the free indices in the Lie algebra,

$$[T^A, T^B] = i f^{ABC} T^C, \qquad (2.5)$$

to lie in the two sectors separately, it is straightforward to deduce

$$f^{ijk} = 0, \qquad f^{ijc} = 0, \qquad (2.6)$$

whence

$$[T^a, T^j] = i f^{ajc} T^c. \qquad (2.7)$$

Using these basic observations and the Casimir definitions,

$$f^{ACD} f^{BCD} = C_A \delta^{AB}, \qquad T^A T^A = C_F I, \qquad (2.8)$$

where the subscript in C_A is not a summed index, one can deduce [47]

$$T^i T^i = \frac{T_F}{N_F} N_A^d I, \qquad T^a T^a = \left[C_F - \frac{T_F}{N_F} N_A^d \right] I$$

$$C_A \delta^{ab} = f^{acd} f^{bcd} + 2 f^{acj} f^{bcj}, \qquad C_A \delta^{ij} = f^{icd} f^{jcd},$$

$$f^{abc} f^{abc} = [N_A^o - 2N_A^d] C_A$$

$$f^{iab} f^{iab} = N_A^d C_A, \qquad f^{acj} f^{bcj} = \frac{N_A^d}{N_A^o} C_A \delta^{ab},$$

$$f^{acd} f^{bcd} = \frac{[N_A^o - 2N_A^d]}{N_A^o} C_A \delta^{ab}. \tag{2.9}$$

In addition, the Jacobi identity

$$0 = f^{ABE} f^{CDE} + f^{BCE} f^{ADE} + f^{CAE} f^{BDE} \tag{2.10}$$

implies

$$f^{apq} f^{bpr} f^{cqr} = \frac{[N_A^o - 3N_A^d]}{2N_A^o} C_A f^{abc},$$

$$f^{apq} f^{bpi} f^{cqi} = \frac{N_A^d}{2N_A^o} C_A f^{abc}$$

$$f^{ipq} f^{bpr} f^{cqr} = \frac{[N_A^o - 2N_A^d]}{2N_A^o} C_A f^{ibc},$$

$$f^{ipq} f^{bpj} f^{cqj} = \frac{N_A^d}{N_A^o} C_A f^{ibc}, \tag{2.11}$$

for the MAG where the covariant derivative D_μ^{ab} acting on the off-diagonal sector is, for instance,

$$(D_\mu A_\nu)^a = \partial_\mu A_\nu^a - g f^{abi} A_\mu^i A_\nu^b,$$
$$(D_\mu c)^a = \partial_\mu c^a - g f^{abi} A_\mu^i c^b, \tag{2.15}$$

and α is the gauge parameter for the off-diagonal sector. It is not to be confused with a similar parameter used in the canonical linear covariant gauge fixing. The other gauge fixing parameter, $\bar{\alpha}$, is the parameter associated with the diagonal sector. It is included here for completeness but throughout it will be set to zero [10–15] so that the diagonal gluons are in the Landau gauge. In addition c^i and c^a are the Faddeev-Popov ghosts associated with the diagonal and off-diagonal sectors and g is the coupling constant. For the Curci-Ferrari gauge,

$$F[A_\mu^A] = \partial^\mu A_\mu^A + \frac{\alpha}{2} b^A - \frac{\alpha}{4} g f^{ABC} \bar{c}^B c^C, \tag{2.16}$$

with $\bar{\alpha} = \alpha$ and b^A is the Nakanishi-Lautrup field for the respective gauges, [15,40]. Although we have already

where we note that here we briefly use p, q and r to denote off-diagonal indices. All these relations were required for the evaluation of the two-loop vertex functions.

As we will be considering two gauges in this article, we note that the general form of the QCD Lagrangian is

$$L = -\frac{1}{4} G_{\mu\nu}^A G^{A\mu\nu} + i\bar{\psi} \not{D} \psi + L_{\text{gf}}, \tag{2.12}$$

with ψ representing N_f flavors of massless quarks and

$$L_{\text{gf}} = -\frac{1}{2\alpha} F[A_\mu^a]^2 - \frac{1}{2\bar{\alpha}} F[A_\mu^i]^2 + \bar{c}^A \left(\frac{\delta F[A_{U\mu}]}{\delta U} \right)^{AB} c^B, \tag{2.13}$$

where $F[A_\mu]$ is the functional of the gauge field whose explicit forms define the different gauges, $A_{U\mu}$ is the gauge field under a general gauge transformation U and c^A and $\bar{c}^A$ are the Faddeev-Popov ghosts. In our case we have

$$F[A_\mu^A] = \begin{cases} (D^\mu A_\mu)^a + \frac{1}{2}\alpha b^a - \frac{1}{2}\alpha g f^{abi} \bar{c}^b c^i - \frac{1}{4}\alpha g f^{abc} \bar{c}^b c^c & \text{if } A = a \\ \frac{1}{\bar{\alpha}} \partial^\mu A_\mu^i & \text{if } A = i \end{cases} \tag{2.14}$$

eliminated b^i in the MAG as the diagonal sector has a simple Abelian structure. From these functionals it is apparent that in the limit where the diagonal fields in the MAG are nullified then the Curci-Ferrari gauge fixing condition emerges if one identifies the off-diagonal indices with those of the full color group.

The first functional leads to the Lagrangian [15],

$$L^{\text{MAG}} = -\frac{1}{4} G_{\mu\nu}^a G^{a\mu\nu} - \frac{1}{4} G_{\mu\nu}^i G^{i\mu\nu} + i\bar{\psi} \not{D} \psi + L_{\text{gf}}^{\text{MAG}}. \tag{2.17}$$

The first two terms derive from the square of the field strength and their sum is gauge invariant. There is no cross term due to (2.3). We have isolated the gauge fixing term $L_{\text{gf}}^{\text{MAG}}$. In a linear covariant gauge, the corresponding term contains the gauge fixing condition and the consequent ghost Lagrangian. For the MAG the situation is the same but the actual Lagrangian is more complicated since [10–15]

$$L_{\text{gf}}^{\text{MAG}} = -\frac{1}{2\alpha}(\partial^\mu A_\mu^a)^2 - \frac{1}{2\bar\alpha}(\partial^\mu A_\mu^i)^2 + \bar{c}^A \partial^\mu \partial_\mu c^A + g\left[f^{abC}A_\mu^a\bar{c}^C\partial^\mu c^b - \frac{1}{\alpha}f^{abk}\partial^\mu A_\mu^a A_\nu^b A^{k\nu} - f^{abk}\partial^\mu A_\mu^a c^b\bar{c}^k\right.$$

$$\left. -\frac{1}{2}f^{abc}\partial^\mu A_\mu^a\bar{c}^b c^c - 2f^{abk}A_\mu^k\bar{c}^a\partial^\mu\bar{c}^b - f^{abk}\partial^\mu A_\mu^k\bar{c}^b c^c\right] + g^2\left[f_d^{acbd}A_\mu^a A^{b\mu}\bar{c}^c c^d - \frac{1}{2\alpha}f_o^{akbl}A_\mu^a A^{b\mu}A_\nu^k A^{l\nu}\right.$$

$$+ f_o^{adcj}A_\mu^a A^{j\mu}\bar{c}^c c^d - \frac{1}{2}f_o^{ajcd}A_\mu^a A^{j\mu}\bar{c}^c c^d + f_o^{ajcl}A_\mu^a A^{j\mu}\bar{c}^c c^l + f_o^{alcj}A_\mu^a A^{j\mu}\bar{c}^c c^l - f_o^{cjdi}A_\mu^i A^{j\mu}\bar{c}^c c^d$$

$$-\frac{\alpha}{4}f_d^{abcd}\bar{c}^a\bar{c}^b c^c c^d - \frac{\alpha}{8}f_o^{abcd}\bar{c}^a\bar{c}^b c^c c^d + \frac{\alpha}{8}f_o^{acbd}\bar{c}^a\bar{c}^b c^c c^d + \frac{\alpha}{4}f^{albc}\bar{c}^a\bar{c}^b c^c c^l$$

$$\left. -\frac{\alpha}{4}f_o^{albc}\bar{c}^a\bar{c}^b c^c c^l + \frac{\alpha}{2}f_o^{akbl}\bar{c}^a\bar{c}^b c^k c^l\right] \tag{2.18}$$

after eliminating b^a where we have introduced the short-hand notation

$$f_d^{ABCD} = f^{iAB}f^{iCD}, \qquad f_o^{ABCD} = f^{eAB}f^{eCD} \tag{2.19}$$

and

$$f^{ABCD} = f_d^{ABCD} + f_o^{ABCD} \tag{2.20}$$

for the quartic interaction terms. Hence, the Jacobi identity is

$$f^{ABCD} + f^{ACDB} + f^{ADBC} = 0. \tag{2.21}$$

As noted in [47] the gauge fixed part of the MAG Lagrangian is generated automatically via a computer algebra routine from the BRST variation of the defining functional. This is to ensure that definitions and conventions are correctly implemented without error as well as to be confident that the resulting Feynman rules are derived correctly using symbolic manipulation. While the form of (2.18) is large, we have endeavored to condense the structure to save space. However, the nature of the MAG with the split in the color group means that L^{MAG} cannot be fully reduced to a form which involves only the general indices A. For the Curci-Ferrari gauge using the second functional, we have

$$L^{\text{CF}} = -\frac{1}{4}G_{\mu\nu}^A G^{A\mu\nu} + i\bar\psi \slashed{D}\psi + L_{\text{gf}}^{\text{CF}} \tag{2.22}$$

with

$$L_{\text{gf}}^{\text{CF}} = -\frac{1}{2\alpha}(\partial^\mu A_\mu^A)^2 - \bar{c}^A(\partial^\mu D_\mu c)^A$$

$$-\frac{g}{2}f^{ABC}\partial^\mu A_\mu^A\bar{c}^B c^C + \frac{\alpha g^2}{8}f^{ABCD}\bar{c}^A c^B\bar{c}^C c^D. \tag{2.23}$$

While this is a more compact Lagrangian, it is straightforward to check that it is connected with (2.18) in the following way. Setting the diagonal gluon and ghost

formally to zero in (2.18) then both Lagrangians are equivalent with the proviso that the adjoint group indices A of (2.23) are equated with the off-diagonal ones of (2.18). In other words if one takes the formal limit $N_A^d \to 0$ then the Curci-Ferrari gauge emerges from (2.18). This property was noted in [47] for the three-loop $\overline{\text{MS}}$ renormalization group functions but as indicated above, this is also evident from the nature of the gauge fixing. We will exploit this observation later in our computations as a nontrivial check. Unlike the linear covariant gauge both the MAG and Curci-Ferrari gauges have quartic ghost interactions but only the MAG has quartic gluon-ghost interactions.

Next it has been shown that both Lagrangians (2.18) and (2.23) are renormalizable [10–15,40,48–53]. However, from an algebraic renormalization analysis the general structure of the renormalization in the MAG has several subtleties. If we define the renormalization constants via the relationship from bare quantities, denoted by $_\text{o}$, to renormalized ones, we have

$$A_\text{o}^{a\mu} = \sqrt{Z_A}A^{a\mu}, \qquad A_\text{o}^{i\mu} = \sqrt{Z_{A^i}}A^{i\mu}, \qquad c_\text{o}^a = \sqrt{Z_c}c^a,$$

$$\bar{c}_\text{o}^a = \sqrt{Z_c}\bar{c}^a, \qquad c_\text{o}^i = \sqrt{Z_{c^i}}c^i$$

$$\bar{c}_\text{o}^i = \frac{\bar{c}^i}{\sqrt{Z_{c^i}}}, \qquad \psi_\text{o} = \sqrt{Z_\psi}\psi, \qquad g_\text{o} = \mu^\epsilon Z_g g,$$

$$\alpha_\text{o} = Z_\alpha^{-1}Z_A\alpha, \qquad \bar\alpha_\text{o} = Z_{\alpha^i}^{-1}Z_{A^i}\bar\alpha. \tag{2.24}$$

Notationally we include a superscript i on the diagonal fields in the various labels on a renormalization constant and understand that there is no summation over this index. For the most part the relation of the bare to renormalized quantity takes its canonical form. However, in order to ensure that the renormalization is consistent with the Slavnov-Taylor identities derived from the BRST symmetry in the MAG, the renormalization of the diagonal ghost, c^i, and its anti-ghost is different as indicated, [15]. The upshot is that one cannot deduce Z_{c^i} from the diagonal ghost 2-point function. To understand this the renormalization constant associated with the off-diagonal ghost 2-point function is given by the product of the

renormalization constants deriving from the external fields. From (2.24) this is clearly Z_c. However, for the diagonal ghost the analogous product of the wave function renormalization constants for the diagonal ghost and anti-ghost is unity, [15]. In other words the diagonal ghost 2-point function is finite and Z_{c^i} can only be deduced from another Green's function which has to be a 3-point function. Moreover, it has to be a vertex which has strictly only one diagonal ghost or anti-ghost. In [47] we used the $A_\mu^a \bar{c}^i c^b$ vertex for this renormalization. As the vertices are ordinarily used to extract the coupling constant renormalization this means that to determine the lth-loop anomalous dimension for c^i one has to renormalize the $A_\mu^a \bar{c}^i c^b$ vertex at the $(l+1)$th order, [15,47]. This is on the assumption that the coupling constant renormalization constant has already been set in a particular scheme. The other feature from the algebraic renormalization analysis is that Z_{A^i} is in effect the same as the coupling constant renormalization, [15]. As was noted in [15,47] this suggests a particular similarity with the background field gauge developed in [41–46] where the β function is given by the background gluon

wave function renormalization. More importantly for our MOM analysis the focus of our computations will be on computing the renormalization constants for the off-diagonal fields, and thence the coupling constant renormalization for the vertices defining a MOM scheme, as these are not determined from any Slavnov-Taylor identity.

As we will be concentrating on the higher-order renormalization of QCD in the MAG we need to review the relevant properties of the renormalization group equation. First, we recall the definition of the renormalization group functions for the fields, denoted generically by ϕ, and α are

$$\gamma_\phi(a, \alpha) = \mu \frac{\partial}{\partial \mu} \ln Z_\phi, \qquad \gamma_\alpha(a, \alpha) = \frac{\mu}{\alpha} \frac{\partial \alpha}{\partial \mu}. \qquad (2.25)$$

With

$$\mu \frac{\partial}{\partial \mu} = \beta(a, \alpha) \frac{\partial}{\partial a} + \alpha \gamma_\alpha(a, \alpha) \frac{\partial}{\partial \alpha}, \qquad (2.26)$$

we have

$$\gamma_A(a, \alpha) = \beta(a, \alpha) \frac{\partial}{\partial a} \ln Z_A + \alpha \gamma_\alpha(a, \alpha) \frac{\partial}{\partial \alpha} \ln Z_A$$

$$\gamma_\alpha(a, \alpha) = \left[\beta(a, \alpha) \frac{\partial}{\partial a} \ln Z_\alpha - \gamma_A(a, \alpha) \right] \left[1 - \alpha \frac{\partial}{\partial \alpha} \ln Z_\alpha \right]^{-1}$$

$$\gamma_{A^i}(a, \alpha) = \beta(a, \alpha) \frac{\partial}{\partial a} \ln Z_{A^i} + \alpha \gamma_\alpha(a, \alpha) \frac{\partial}{\partial \alpha} \ln Z_{A^i}$$

$$\gamma_c(a, \alpha) = \beta(a, \alpha) \frac{\partial}{\partial a} \ln Z_c + \alpha \gamma_\alpha(a, \alpha) \frac{\partial}{\partial \alpha} \ln Z_c$$

$$\gamma_{c^i}(a, \alpha) = \beta(a, \alpha) \frac{\partial}{\partial a} \ln Z_{c^i} + \alpha \gamma_\alpha(a, \alpha) \frac{\partial}{\partial \alpha} \ln Z_{c^i}$$

$$\gamma_\psi(a, \alpha) = \beta(a, \alpha) \frac{\partial}{\partial a} \ln Z_\psi + \alpha \gamma_\alpha(a, \alpha) \frac{\partial}{\partial \alpha} \ln Z_\psi, \qquad (2.27)$$

where $a = g^2/(16\pi^2)$. Some clarification is perhaps in order for the forms of $\gamma_A(a, \alpha)$ and $\gamma_\alpha(a, \alpha)$. If one was working in a linear covariant gauge such as the Landau gauge the gauge parameter does not get renormalized and $Z_\alpha = 1$ in our conventions. Therefore the second equation of (2.27) would reflect the textbook situation if one formally sets $Z_\alpha = 1$. In nonlinear covariant gauges such as the Curci-Ferrari gauge and the MAG $Z_\alpha \neq 1$. Therefore one has to be careful in deriving (2.27) from (2.26) in order to express $\gamma_A(a, \alpha)$ and $\gamma_\alpha(a, \alpha)$ purely in terms of their respective renormalization constants Z_A and Z_α. In (2.27) we have included gauge parameter dependence in the β function, $\beta(a, \alpha)$, because in mass dependent renormalization schemes, such as the MOM ones, the β function is not independent of the gauge parameter. In mass-independent schemes such as $\overline{\text{MS}}$ the β function is independent of α,

[54]. Also the definition of the renormalization group function for α is more involved than in a linear covariant gauge because by contrast in the MAG and Curci-Ferrari gauge Z_α is not equivalent to Z_A.

In providing (2.27) we note that these are valid in any renormalization scheme. However, the parameters which the renormalization group functions depend on are defined with respect to a scheme which here will either be a MOM scheme or the $\overline{\text{MS}}$ scheme. As one of our aims is to establish the three-loop MOM renormalization group functions we must record the relation between parameters in different schemes and then the way of deriving the three-loop MOM results from the two-loop vertex function renormalization. For the first part of this exercise, the relation between the coupling constant and gauge parameter in two schemes is given by

$$g_{\text{MOMi}}(\mu) = \frac{Z_g^{\overline{\text{MS}}}}{Z_g^{\text{MOMi}}} g_{\overline{\text{MS}}}(\mu),$$

$$\alpha_{\text{MOMi}}(\mu) = \frac{Z_A^{\overline{\text{MS}}} Z_\alpha^{\text{MOMi}}}{Z_A^{\text{MOMi}} Z_\alpha^{\overline{\text{MS}}}} \alpha_{\overline{\text{MS}}}(\mu), \qquad (2.28)$$

where MOMi indicates one of the MOM schemes. In practical terms, one has to be careful in deriving the relationship between the parameters since the renormalization constants are functions of the parameters in the scheme defined by the label. Therefore, one constructs the perturbative relation order by order in the coupling constant expansion to ensure that there are no singularities in the regularizing parameter. Throughout, we dimensionally regularize the theory in $d = 4 - 2\epsilon$ dimensions where ϵ is the regulator. Once these mappings of the parameters between the schemes have been determined, we can define the conversion functions $C_\phi^{\text{MOMi}}(a, \alpha)$, where ϕ indicates the appropriate field, and $C_\alpha^{\text{MOMi}}(a, \alpha)$. These are at the core of the three-loop MOM renormalization group construction and are defined by

$$C_\phi^{\text{MOMi}}(a, \alpha) = \frac{Z_\phi^{\text{MOMi}}}{Z_\phi^{\overline{\text{MS}}}} \qquad (2.29)$$

for the fields and

$$C_\alpha^{\text{MOMi}}(a, \alpha) = \frac{Z_\alpha^{\text{MOMi}} Z_A^{\overline{\text{MS}}}}{Z_\alpha^{\overline{\text{MS}}} Z_A^{\text{MOMi}}} \qquad (2.30)$$

for the gauge parameter. As has been our convention [37], the variables a and α are $\overline{\text{MS}}$ parameters. In (2.29) and (2.30) the coupling constant and gauge parameter dependence has been omitted for reasons of space. In each the dependence is given by

$$Z_\phi^{\text{MOMi}} = Z_\phi^{\text{MOMi}}(a_{\text{MOMi}}(a, \alpha), \alpha_{\text{MOMi}}(a, \alpha))$$
$$Z_\alpha^{\text{MOMi}} = Z_\alpha^{\text{MOMi}}(a_{\text{MOMi}}(a, \alpha), \alpha_{\text{MOMi}}(a, \alpha)) \qquad (2.31)$$

because we have chosen the $\overline{\text{MS}}$ scheme as the reference scheme. In computing the explicit forms for the conversion functions from the renormalization constants at a particular order one has to use the relation between each of the parameters which was determined at the previous order. This iterative procedure then ensures that the conversion functions are finite with respect to ϵ. With these the formal relation of the renormalization group functions in different schemes is

$$\beta^{\text{MOMi}}(a_{\text{MOMi}}, \alpha_{\text{MOMi}}) = \left[\beta^{\overline{\text{MS}}}(a_{\overline{\text{MS}}}) \frac{\partial a_{\text{MOMi}}}{\partial a_{\overline{\text{MS}}}} + \alpha_{\overline{\text{MS}}} \gamma_\alpha^{\overline{\text{MS}}}(a_{\overline{\text{MS}}}, \alpha_{\overline{\text{MS}}}) \frac{\partial a_{\text{MOMi}}}{\partial \alpha_{\overline{\text{MS}}}} \right]_{\overline{\text{MS}} \to \text{MOMi}}$$

$$\gamma_\phi^{\text{MOMi}}(a_{\text{MOMi}}, \alpha_{\text{MOMi}}) = [\gamma_\phi^{\overline{\text{MS}}}(a_{\overline{\text{MS}}}) + \beta^{\overline{\text{MS}}}(a_{\overline{\text{MS}}}) \frac{\partial}{\partial a_{\overline{\text{MS}}}} \ln C_\phi^{\text{MOMi}}(a_{\overline{\text{MS}}}, \alpha_{\overline{\text{MS}}})$$

$$+ \alpha_{\overline{\text{MS}}} \gamma_\alpha^{\overline{\text{MS}}}(a_{\overline{\text{MS}}}, \alpha_{\overline{\text{MS}}}) \frac{\partial}{\partial \alpha_{\overline{\text{MS}}}} \ln C_\phi^{\text{MOMi}}(a_{\overline{\text{MS}}}, \alpha_{\overline{\text{MS}}})]_{\overline{\text{MS}} \to \text{MOMi}}, \qquad (2.32)$$

where the subscript mapping on the parentheses indicates that after the object is computed in $\overline{\text{MS}}$ variables, they are mapped to MOMi ones, [55].

III. COMPUTATIONAL SETUP

Having outlined the relevant aspects of the renormalization group we now turn to the practical aspects of the calculation. As in the previous computation, [37], we focus on the three vertices at the symmetric point which will define the three MOM schemes. They are given by

$$\langle A_\mu^a(p) A_\nu^b(q) A_\sigma^c(r) \rangle |_{p^2 = q^2 = -\mu^2} = f^{abc} \Sigma_{\mu\nu\sigma}^{ggg}(p, q) |_{p^2 = q^2 = -\mu^2}$$
$$\langle c^a(p) \bar{c}^b(q) A_\sigma^c(r) \rangle |_{p^2 = q^2 = -\mu^2} = f^{abc} \Sigma_\sigma^{ccg}(p, q) |_{p^2 = q^2 = -\mu^2}$$
$$\langle \psi(p) \bar{\psi}(q) A_\sigma^c(r) \rangle |_{p^2 = q^2 = -\mu^2} = T^c \Sigma_\sigma^{q\bar{q}g}(p, q) |_{p^2 = q^2 = -\mu^2}, \qquad (3.1)$$

where p, q and r are external momenta and we choose the third momentum to be the dependent one,

$$r = -p - q, \qquad (3.2)$$

with

$$p^2 = q^2 = r^2 = -\mu^2 \qquad (3.3)$$

defining the symmetric point giving

$$pq = \frac{1}{2}\mu^2. \qquad (3.4)$$

The color group tensors for each vertex have been factored off from the Lorentz structure $\Sigma_{\mu_1 \dots \mu_n}^V(p, q)|_{p^2 = q^2 = -\mu^2}$. We note that (3.1) will be used for the calculations in both gauges. For the Curci-Ferrari case, as there are no diagonal indices, the global index A used in (2.16) can be

unambiguously identified with the index a. The absence of the totally symmetric tensor d^{abc} at least in our two-loop decomposition derives from Furry's theorem and its consequences in massless QCD. Here V indicates the appropriate vertex and n is unity for the quark and ghost vertices but 3 for the triple off-diagonal gluon vertex. The restriction to the symmetric point is included as the Lorentz structure of the full vertex away from this point is different. Both

have been discussed in previous work, [37,56]. For the MAG case the explicit forms of the tensors into which each vertex is decomposed is given in [37] and we will use the same basis here for consistency. More specifically, the Lorentz amplitude for each vertex is decomposed into the full basis of tensors, where the coefficients of each Lorentz tensor corresponds to the scalar Feynman integrals within the Green's functions, as

$$\Sigma^{\mathrm{ggg}}_{\mu\nu\sigma}(p,q)|_{p^2=q^2=-\mu^2} = \sum_{k=1}^{14} \mathcal{P}^{\mathrm{ggg}}_{(k)\mu\nu\sigma}(p,q)(\Sigma^{\mathrm{ggg}}_{(k)}(p,q)|_{p^2=q^2=-\mu^2})$$

$$\Sigma^{\mathrm{ccg}}_{\sigma}(p,q)|_{p^2=q^2=-\mu^2} = \sum_{k=1}^{2} \mathcal{P}^{\mathrm{ccg}}_{(k)\sigma}(p,q)(\Sigma^{\mathrm{ccg}}_{(k)}(p,q)|_{p^2=q^2=-\mu^2})$$

$$\Sigma^{\mathrm{qqg}}_{\sigma}(p,q)|_{p^2=q^2=-\mu^2} = \sum_{k=1}^{6} \mathcal{P}^{\mathrm{qqg}}_{(k)\sigma}(p,q)(\Sigma^{\mathrm{qqg}}_{(k)}(p,q)|_{p^2=q^2=-\mu^2}), \tag{3.5}$$

where k labels a particular tensor. To extract the perturbative expansion for the scalar amplitudes we use the projection method which was discussed in [37]. Briefly, to determine a particular amplitude, one multiplies each vertex function by a specific linear combination of tensors from the basis,

$$f^{\mathrm{abc}}\Sigma^{\mathrm{ggg}}_{(k)}(p,q) = \mathcal{M}^{\mathrm{ggg}}_{kl}(\mathcal{P}^{\mathrm{ggg}\mu\nu\sigma}_{(l)}(p,q)\langle A^a_\mu(p)A^b_\nu(q)A^c_\sigma(r)\rangle)|_{p^2=q^2=-\mu^2}$$

$$f^{bac}\Sigma^{\mathrm{ccg}}_{(k)}(p,q) = \mathcal{M}^{\mathrm{ccg}}_{kl}(\mathcal{P}^{\mathrm{ccg}\sigma}_{(l)}(p,q)\langle c^a(p)\bar{c}^b(q)A^c_\sigma(r)\rangle)|_{p^2=q^2=-\mu^2}$$

$$T^c\Sigma^{\mathrm{qqg}}_{(k)}(p,q) = \mathcal{M}^{\mathrm{qqg}}_{kl}(\mathcal{P}^{\mathrm{qqg}\sigma}_{(l)}(p,q)\langle \psi(p)\bar{\psi}(q)A^c_\sigma(r)\rangle)|_{p^2=q^2=-\mu^2}, \tag{3.6}$$

where $\mathcal{M}^V_{kl}$ is a matrix whose elements are rational polynomials in d and whose kth row is the linear combination required for the kth amplitude. This matrix is given in [37] for each vertex. The color group dependence has been included here to balance the color indices on the right-hand side. As noted earlier to two loops the left-hand side reflects the actual structure. If it were not the case then we would have to introduce a color projection. In performing the Lorentz projection the Lorentz integrals within each vertex function become scalar integrals and the resulting numerator scalar products are rewritten as far as possible in terms of the propagators. The reason for this is that we will use the Laporta algorithm, [57], to perform the computations. This is a method which derives integration by parts relations between scalar Feynman integrals and then solves them in terms of a relatively small set of master integrals. The values of these masters are determined by direct methods. In rewriting the scalar products as indicated this may produce an irreducible numerator. One feature of the Laporta algorithm, [57], is that it can handle such irreducible cases systematically. For our specific 3-point symmetric vertex computation there is one topology in the one-loop integral family which is the triangle graph. At two loops there are two topologies in that integral family. One is

the two-loop nonplanar vertex and the other is the ladder graph. These are illustrated in Fig. 1. If one was away from the symmetric point then there would be at most two additional ladder topologies, [56], which correspond to two rotations of the final graph.

In terms of practicalities, such a computation can only be managed within a reasonable amount of time with the use of computer algebra packages. The main tool for handling the large amounts of tedious algebra is FORM, [58], and its threaded version TFORM, [59]. The Feynman graphs are generated using the QGRAF package [60] and then converted into FORM notation where all the color and Lorentz indices are added. The number of graphs computed for each vertex is given in Table I for the MAG and Table II for the Curci-Ferrari gauge. For the implementation of the Laporta algorithm we have chosen to use the REDUZE package, [61], which is written in GINAC, [62]. One useful feature of REDUZE is that the reduction to master integrals can be extracted from the database of relations REDUZE creates in FORM syntax. This has allowed us to set up an automatic computation whereby the relevant integrals from the database are included within a FORM module. The remaining general tasks are the evaluation and inclusion of the master integrals and the renormalization. For the former all the
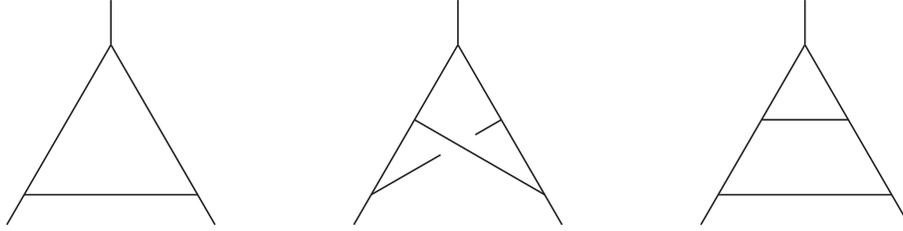
FIG. 1.   Integral families at one and two loops for the symmetric point.

one- and two-loop masters are already known to the order in ϵ required for the two-loop vertex functions to the finite part [63–68]. A complete set for easy reference has been provided in [67] and we use the same notation throughout this article. For several masters the expansion in ϵ is needed to $O(\epsilon^2)$. Ordinarily, for a two-loop renormalization this would not be necessary. However, in the construction of the integration by parts relations spurious poles in ϵ appear which multiply several masters. This requires the extra terms in the master integral ϵ expansion. While we will be discussing general features of the full analytic results later with the explicit expressions being included in attached data files [69], we need to comment on the structure. This is dictated by the expressions for the masters and involve the polylogarithm function $\text{Li}_n(z)$ via the function

$$s_n(z) = \frac{1}{\sqrt{3}} \Im \left[\text{Li}_n \left(\frac{e^{iz}}{\sqrt{3}} \right) \right]. \qquad (3.7)$$

In previous work in other gauges, [70], the final expressions involved the quantity Σ which was defined as the following combination of harmonic polylogarithms

$$\Sigma = \mathcal{H}_{31}^{(2)} + \mathcal{H}_{43}^{(2)} \qquad (3.8)$$

in the notation of [67]. Such quantities are not unrelated to harmonic polylogarithms based on cyclotomic polynomials, [71]. However, it transpires that this object was not independent of another combination of quantities which appear since [68],

$$\Sigma = \frac{1}{36} \psi''' \left(\frac{1}{3} \right) - \frac{2\pi^4}{27} \qquad (3.9)$$

where $\psi(z)$ is the derivative of the logarithm of the Euler Γ function. Therefore, in the expressions in our data files, the object Σ does not formally appear unlike [70]. Of course in numerical results both quantities have the same value. To assist numerical evaluation we note that

$$\zeta_3 = 1.20205690, \qquad \psi'\left(\frac{1}{3}\right) = 10.09559713,$$

$$\psi'''\left(\frac{1}{3}\right) = 488.1838167 \qquad s_2\left(\frac{\pi}{2}\right) = 0.32225882,$$

$$s_2\left(\frac{\pi}{6}\right) = 0.22459602, \qquad s_3\left(\frac{\pi}{2}\right) = 0.32948320$$

$$s_3\left(\frac{\pi}{6}\right) = 0.19259341, \qquad (3.10)$$

where ζ_z is the Riemann zeta function. Finally, as we are performing an automatic symbolic manipulation program, we use the renormalization procedure developed in [72] to extract the renormalization constants for each vertex. Briefly all vertex functions are computed in terms of bare parameters which means the coupling constant and gauge parameter. Their associated counterterms are introduced symbolically after all graphs have been computed and summed by rescaling with the appropriate renormalization constant defined in (2.24).

To extract the MOM renormalization constant from each vertex function additionally requires the wave function renormalization constant of the external fields in the MOM

TABLE I.   Number of Feynman diagrams for each 2- and 3-point function in the MAG.

Green's function	One loop	Two loop	Total
$A_\mu^a A_\nu^b$	6	131	137
$c^a \bar{c}^b$	3	54	57
$\psi \bar{\psi}$	3	81	84
$A_\mu^a A_\nu^b A_\sigma^c$	23	1291	1314
$c^a \bar{c}^b A_\sigma^c$	16	867	883
$\psi \bar{\psi} A_\sigma^c$	5	217	222
Total	56	2641	2697

TABLE II.   Number of Feynman diagrams for each 2- and 3-point function in the Curci-Ferrari gauge.

Green's function	One loop	Two loop	Total
$A_\mu^A A_\nu^B$	3	19	22
$c^A \bar{c}^B$	1	9	10
$\psi \bar{\psi}$	1	6	7
$A_\mu^A A_\nu^B A_\sigma^C$	8	112	120
$c^A \bar{c}^B A_\sigma^C$	3	49	52
$\psi \bar{\psi} A_\sigma^C$	2	33	35
Total	18	228	246

scheme. This is achieved by performing the 2-point function two-loop renormalization of the off-diagonal gluon, ghost and quark fields in each of the MOM schemes. For these we use the MINCER algorithm, [73], which is implemented in FORM, [74]. The number of graphs for each of the 2-point functions is given in Table I for the MAG and those for the Curci-Ferrari gauge are given in Table II. In extracting the wave function and gauge parameter renormalization constants, using the same automatic procedure as [72], we note that the one-loop 2-point functions are renormalized first in the MOM scheme of [38,39] and then the one-loop vertex functions. The latter define the three schemes which are then used to determine the wave function and gauge parameter renormalizations at two loops before these are used to deduce the coupling constant renormalization constants for each of the three MOM schemes. We note that the method to define each MOM scheme is based on the original program of [38,39] and was followed in [37]. For each of the 2-point and vertex function renormalizations at the subtraction point the MOM scheme is defined so that after the renormalization constant has been defined there are no $O(a)$ corrections. For the vertex functions this is qualified by noting that it is the Lorentz channels of the tree level which has no $O(a)$ corrections after renormalization. The non-tree-level vertex structures will have $O(a)$ corrections at the symmetric point. As one check on our computer algebraic programs, we have verified that the two-loop $\overline{\text{MS}}$ coupling constant

renormalization constant of [75,76] correctly emerges from each 3-point vertex function. This completes the description of the technology to compute the 3-point functions at the symmetric point. It now remains to discuss the results.

IV. RESULTS

Before discussing the renormalization group functions and vertex functions, we detail the additional checks on our computations. As the first stage in considering the renormalization of the MAG and Curci-Ferrari gauges beyond that of [37] in MOM schemes, we have determined each vertex function in the $\overline{\text{MS}}$ scheme at the symmetric point. An important check on the computations is that at the symmetric point the divergent terms in ϵ can be minimally subtracted and the resulting renormalization constants agree with those of [47,77]. By this we mean that the wave function renormalization constants associated with the external legs of the respective vertex functions are such that the final renormalization constant corresponding to the coupling constant correctly emerges in agreement with the known two-loop $\overline{\text{MS}}$ result of [1,2,75,76]. An additional check is that the relations between various amplitudes which were observed in [37] at one loop are maintained at two loops. For instance, those of the triple off-diagonal gluon in the MAG are the same as those of the triple gluon in the linear covariant gauge. Thus, at the symmetric point we have checked that the relations

$$\Sigma_{(1)}^{ggg}(p,q)\big|_{p^2=q^2=-\mu^2}^{\overline{\text{MS}}} = \Sigma_{(2)}^{ggg}(p,q)\big|_{p^2=q^2=-\mu^2}^{\overline{\text{MS}}} = -\frac{1}{2}\Sigma_{(3)}^{ggg}(p,q)\big|_{p^2=q^2=-\mu^2}^{\overline{\text{MS}}}$$

$$= -\Sigma_{(4)}^{ggg}(p,q)\big|_{p^2=q^2=-\mu^2}^{\overline{\text{MS}}} = \frac{1}{2}\Sigma_{(5)}^{ggg}(p,q)\big|_{p^2=q^2=-\mu^2}^{\overline{\text{MS}}} = -\Sigma_{(6)}^{ggg}(p,q)\big|_{p^2=q^2=-\mu^2}^{\overline{\text{MS}}}$$

$$\Sigma_{(7)}^{ggg}(p,q)\big|_{p^2=q^2=-\mu^2}^{\overline{\text{MS}}} = 2\Sigma_{(9)}^{ggg}(p,q)\big|_{p^2=q^2=-\mu^2}^{\overline{\text{MS}}} = -2\Sigma_{(11)}^{ggg}(p,q)\big|_{p^2=q^2=-\mu^2}^{\overline{\text{MS}}} = -\Sigma_{(14)}^{ggg}(p,q)\big|_{p^2=q^2=-\mu^2}^{\overline{\text{MS}}}$$

$$\Sigma_{(8)}^{ggg}(p,q)\big|_{p^2=q^2=-\mu^2}^{\overline{\text{MS}}} = -\Sigma_{(13)}^{ggg}(p,q)\big|_{p^2=q^2=-\mu^2}^{\overline{\text{MS}}}$$

$$\Sigma_{(10)}^{ggg}(p,q)\big|_{p^2=q^2=-\mu^2}^{\overline{\text{MS}}} = -\Sigma_{(12)}^{ggg}(p,q)\big|_{p^2=q^2=-\mu^2}^{\overline{\text{MS}}} \tag{4.1}$$

emerge correctly to two loops for the triple off-diagonal gluon vertex. For the off-diagonal ghost vertex there are two amplitudes but the nature of the vertex in the MAG is such that only one is independent. Therefore, we found

$$\Sigma_{(1)}^{ccg}(p,q)\big|_{p^2=q^2=-\mu^2}^{\overline{\text{MS}}} = -\Sigma_{(2)}^{ccg}(p,q)\big|_{p^2=q^2=-\mu^2}^{\overline{\text{MS}}}. \tag{4.2}$$

Finally, for the quark off-diagonal gluon vertex, we have verified that

$$\Sigma_{(2)}^{qqg}(p,q)\big|_{p^2=q^2=-\mu^2}^{\overline{\text{MS}}} = \Sigma_{(5)}^{qqg}(p,q)\big|_{p^2=q^2=-\mu^2}^{\overline{\text{MS}}},$$

$$\Sigma_{(3)}^{qqg}(p,q)\big|_{p^2=q^2=-\mu^2}^{\overline{\text{MS}}} = \Sigma_{(4)}^{qqg}(p,q)\big|_{p^2=q^2=-\mu^2}^{\overline{\text{MS}}} \tag{4.3}$$

are satisfied like the others for all values of α. The amplitudes associated with channels 1 and 6 in the quark-gluon vertex are not related to any of the others. The former corresponds to the tree level vertex and the latter is in a separate partition of spinor space as discussed in [70]. One feature which is apparent in MAG expressions, and those at one loop in [37], is that the amplitudes corresponding to the original Feynman rule are nonsingular in α. Thus, using this channel for the definition of MOM schemes does

not lead to problems in the true definition of the MAG. For the Curci-Ferrari gauge the same relations between the amplitudes hold. For the ghost-gluon vertex this is different from the situation in the linear covariant gauge. In that gauge the ghost-gluon vertex is not antisymmetric since the spacetime derivative in the Lagrangian only acts on one of the ghost fields unlike the Curci-Ferrari gauge. Thus, in the latter the amplitudes are related as given above.

Now that the evaluation of the vertex functions have been established in the $\overline{\text{MS}}$ scheme and the correct renormalization group functions emerge we turn to the situation in the MOM schemes. To summarize we have defined MOMi with respect to the Lorentz channel corresponding to the tree level vertex structure. In other words at the fully symmetric point the coupling constant renormalization constant is chosen such that there are no $O(a)$ corrections in keeping with the ethos of [38,39]. The process is an iterative one. Briefly, at a given loop order all 2-point functions are first rendered finite in MOMi. Then the appropriate MOMi vertex is renormalized at the same loop order. Once equipped with this coupling constant renormalization constant, the subsequent loop order of all the 2-point functions is renormalized in MOMi before repeating the exercise for the coupling constant renormalization. This establishes the MOMi renormalization constants at two loops and then we deduce the various conversion functions to two loops. These are required for going beyond this order to determine the three-loop renormalization group functions ahead of an explicit computation. In order to achieve this, we require the mappings of the parameters between the schemes which are formally defined in (2.28).

There are various checks on the full analytic expressions for these renormalization group functions. The first is that the two-loop results agree with those determined in [37]. The method we used in [37] was to exploit the properties of

the renormalization group. In other words the one-loop vertex function renormalization in the MOM schemes produced the conversion functions which, via the renormalization group formalism, determined the then to be explicitly computed two-loop anomalous dimensions. Therefore using this blind check it is satisfying to record that the explicit computation is in agreement. The other main check is due to the relation the MAG has with the Curci-Ferrari gauge. If one takes the limit of the MAG where the Abelian sector is formally removed, then the remaining Lagrangian involving the off-diagonal fields is equivalent to the massless Curci-Ferrari Lagrangian of [40]. Therefore, the renormalization group functions of the MAG in the $N_A^d/N_A^o \to 0$ limit should agree with those in the Curci-Ferrari gauge in each of the three schemes. This is the case for $\overline{\text{MS}}$, [47]. For the MOMi schemes this is also the situation here since the three-loop MOMi renormalization group functions have been evaluated directly in the Curci-Ferrari gauge. We note that we have taken the $N_A^d/N_A^o \to 0$ limit in the MAG and verified that both computations are consistent. The final check rests in the fact that the double poles in ϵ in the renormalization constants in the various MOM schemes are not independent and are determined by the simple pole at one loop. That the double poles are in agreement in both gauges indicates that those graphs with subgraph divergences have been correctly treated within the symbolic manipulation programs we have developed. Finally, the relations between the amplitudes in (4.1), (4.2) and (4.3) for $\overline{\text{MS}}$ in both gauges also hold after renormalization in the MOM schemes too.

Having compiled all the renormalization group functions in each of the three schemes, it is interesting to make an initial comparison of the size of the corrections. As a simple benchmark we consider the three-loop MAG β functions in each of the four schemes for $\alpha = 0$. We have, for instance,

$$
\begin{aligned}
\beta^{\overline{\text{MS}}}(a,0) = {} & [0.666667N_f - 11.000000]a^2 + [12.666667N_f - 102.000000]a^3 \\
& + [-6.018518N_f^2 + 279.611111N_f - 1428.500000]a^4 + O(a^5)
\end{aligned}
$$

$$
\begin{aligned}
\beta^{\text{MOMggg}}(a,0) = {} & [0.666667N_f - 11.000000]a^2 + [12.666667N_f - 93.608510]a^3 \\
& + [-2.658115N_f^3 + 54.791594N_f^2 + 401.565562N_f - 3543.358228]a^4 + O(a^5)
\end{aligned}
$$

$$
\begin{aligned}
\beta^{\text{MOMh}}(a,0) = {} & [0.666667N_f - 11.000000]a^2 + [12.666667N_f - 108.000000]a^3 \\
& + [-25.035332N_f^2 + 674.085832N_f - 2991.050472]a^4 + O(a^5)
\end{aligned}
$$

$$
\begin{aligned}
\beta^{\text{MOMq}}(a,0) = {} & [0.666667N_f - 11.000000]a^2 + [12.666667N_f - 96.936557]a^3 \\
& + [-22.587812N_f^2 + 627.275918N_f - 2266.490127]a^4 + O(a^5),
\end{aligned} \tag{4.4}
$$

where the $\overline{\text{MS}}$ results were given originally in [1,2,74,76,78]. At two loops there is not a significant departure from the $\overline{\text{MS}}$ value of the comparable term. The major difference is in the three-loop term where, for instance, in the Yang-Mills case the coefficient in each

of the three MOM schemes is roughly twice that of the three-loop $\overline{\text{MS}}$ value, while for mass-independent renormalization schemes the three-loop term is the first point where scheme dependence will arise. By contrast in mass dependent schemes, which includes the MOM cases, this

will occur at the previous order as is evident in (4.4). What is not predictable prior to an explicit computation is the magnitude of any correction. While the large difference with $\overline{\text{MS}}$ is consistent within the three schemes, a better comparison might be with a physical quantity which we will consider later. From [70] comparing the same N_f independent Landau gauge coefficient in the three-loop MOM β functions the MOMggg scheme coefficient of [70] is roughly the same as the $\overline{\text{MS}}$ value but the MOMq and MOMh values are more in line with the analogous scheme in the MAG. This is slightly surprising as naively the expectation might have been that all three MOM schemes in the MAG would have been similar to the MOM schemes of [70].

While the β functions give some insight into the size of the corrections in various schemes, the effect of the higher-order corrections on the structure of the vertex functions is also of interest at the symmetric point. We have chosen to illustrate this graphically. So in order to construct plots of the vertex functions at the symmetric point with respect to a scale we first convert the coupling constant to its explicit scale dependence. We introduce the partial coupling constants $a_l(\mu, \Lambda)$, where l is the loop order, which are given by solving the β function as a differential equation for the coupling constant. We have

$$a_1(\mu, \Lambda) = \frac{1}{b_0 L}, \qquad a_2(\mu, \Lambda) = \frac{1}{b_0 L}\left[1 - \frac{b_1 \ln(L)}{b_0^2 L}\right]$$

$$a_3(\mu, \Lambda) = \frac{1}{b_0 L}\left[1 - \frac{b_1 \ln(L)}{b_0^2 L} + [b_1^2[\ln^2(L)\right.$$
$$\left. - \ln(L) - 1] + b_0 b_2]\frac{1}{b_0^4 L^2}\right], \qquad (4.5)$$

where

$$L = \ln\left(\frac{\mu^2}{\Lambda^2}\right) \qquad (4.6)$$

and the β-function coefficients are defined by

$$\beta(a, 0) = -\sum_{n=0}^{\infty} b_n a^{n+1}. \qquad (4.7)$$

Here Λ is the scale associated with the constant of integration. It has different values depending on the number of quark flavors but in this analysis we will leave it as a free parameter and not fix it to any specific value. For the higher-order forms of $a_l(\mu, \Lambda)$ in (4.5) we have chosen to use the versions given in [79] and for this analysis we will concentrate on the $\alpha = 0$ case as this is the value which defines the MAG. We will use $a_l(\mu, \Lambda)$ at the lth loop to construct the truncated vertex functions and compare them. Therefore, if we write

$$\Sigma_{(k)}^V(p, q)\Big|_{p^2 = q^2 = -\mu^2} = \sum_{n=0}^{\infty} \Sigma_{(k)n}^V a^n \qquad (4.8)$$

for each vertex V and channel k then we define the truncated vertex functions $T_{k,l}^V$ at the symmetric point by

$$T_{k,l}^V = \sum_{n=0}^{l} \Sigma_{(k)n}^V (a_l(\mu, \Lambda))^n, \qquad (4.9)$$

where l is the number of loops at which the truncation occurs. Having defined the truncated vertex functions we will give plots for $l = 1$ and 2 in the $\overline{\text{MS}}$ scheme at the symmetric point for the channels corresponding to the tree level vertex structures. This is because for the MOM schemes the symmetric point vertex functions are by definition a constant for all l for the same channels. Our plots are given in Fig. 2, and we have selected a representative for each vertex and one of four values of N_f. This is primarily because overall the plots are very similar in form to the ones not given. In general, the behavior from one to two loops is the same in that at higher values of N_f, there is little difference between one and two loops, while the $N_f = 3$ plots suggest a larger discrepancy. Quantifying the difference, it transpires that over the range of $x = \mu/\Lambda$ given in the figures, there is only a change of 1%. This is as expected as we are well within the range of perturbative reliability. Moreover, comparing these corrections with comparable plots, [56], the order of the corrections is similar if not marginally better than those for the linear covariant gauge fixing. This is reassuring in light of the full off-shell two-loop analysis of [56] where it was shown that the two-loop corrections were not significantly different from one loop for all ranges of the external momenta away from the symmetric point. The plots in Fig. 2 represent the diagonal section across the $(p^2/\mu^2, q^2/\mu^2)$ plane. In [56] the vertex functions in a linear covariant gauge were determined over this whole plane.

The situation in the Curci-Ferrari gauge follows a similar pattern. However, as the main difference in that gauge compared with the linear covariant gauge is the nature of the ghost-gluon vertex we focus our discussion on the corresponding amplitudes. We have illustrated these in Fig. 3 for a range of N_f in the $\overline{\text{MS}}$ scheme. Concerning the normalization we have chosen in this case to plot the channel 1 amplitude multiplied by a factor of 2. This is to allow us to compare with a similar plot for the linear covariant gauge given in [70]. A similar picture emerges in that for larger values of N_f the one and two-loop corrections are effectively the same. While the discrepancy looks large for smaller values of N_f at any specific value of x, the variation is no more than 0.5%. If we compare the Curci-Ferrari gauge ghost-gluon vertices with the off-diagonal ghost-gluon vertex in the MAG we see that at high
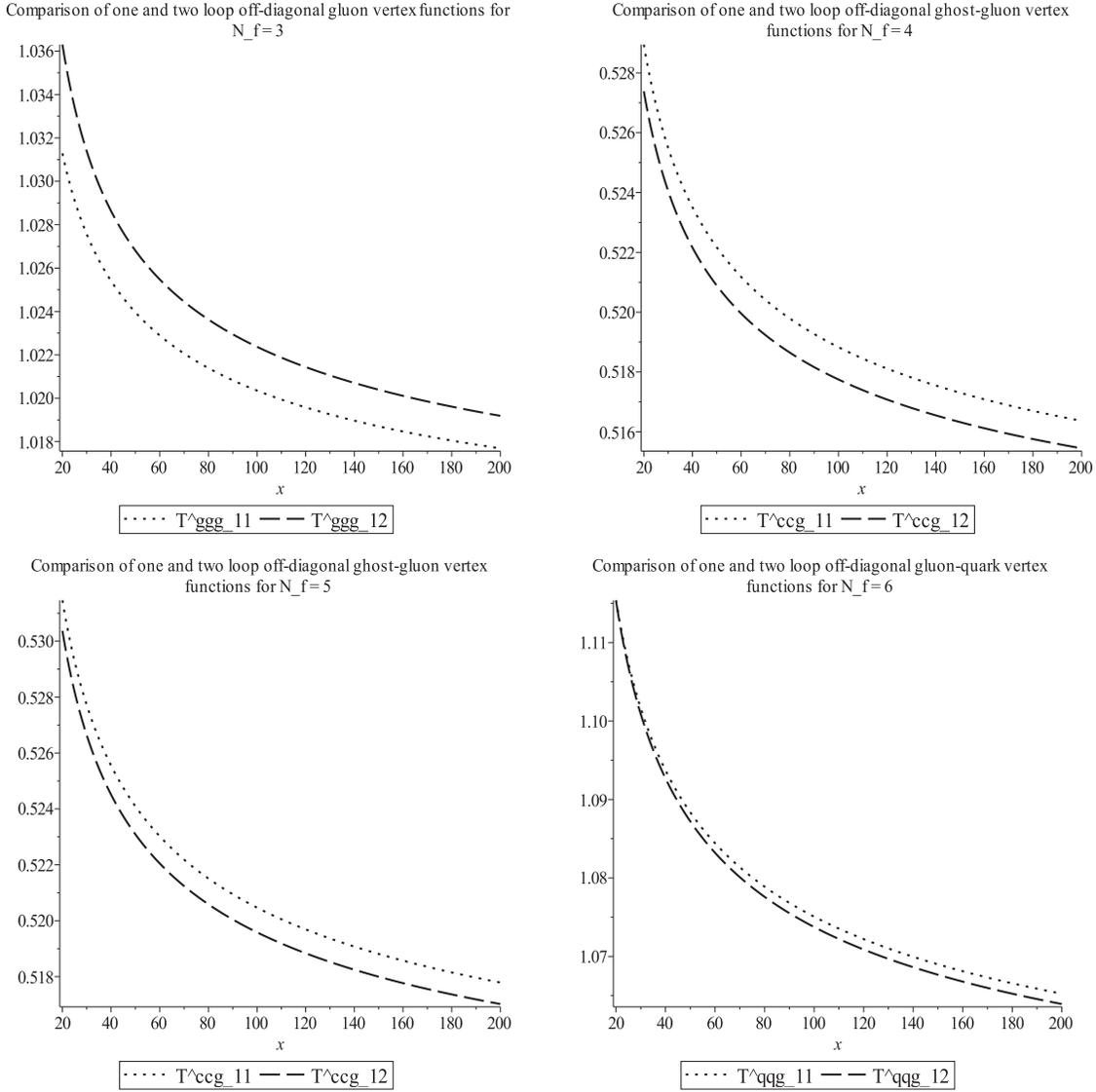
FIG. 2.   Comparison of various $\overline{\text{MS}}$ MAG vertex functions for different values of N_f.

momenta they are virtually indistinguishable. Where there is any difference, it is at lower values of x. This is not unexpected as in effect at large energy the one-loop piece of each vertex would be dominant. Moreover, the one-loop running of the coupling constant is both scheme and gauge independent.

As the $\overline{\text{MS}}$ results give an indication of the effect of the higher-order corrections and the small changes that the two-loop contributions make, the situation with the MOM schemes cannot be seen given that we are focused at the symmetric point. Instead it seems appropriate to consider a physical quantity and compare values for it in the different schemes. In [80] the flavor nonsinglet R ratio was evaluated in the MOM schemes of Celmaster and Gonsalves for the Landau gauge at three loops and compared with the $\overline{\text{MS}}$ scheme form, [81–87]. Therefore, we have repeated that exercise for the MOM schemes of the MAG. First, we

recall the notation used in [80] and define the R ratio in scheme $\mathcal{S}$ by

$$R^{\mathcal{S}}(s) = N_F \left(\sum_f Q_f^2 \right) r^{\mathcal{S}}(s), \qquad (4.10)$$

where N_F is the dimension of the fundamental representation, Q_f is the charge of the active number of quarks, s is the center of mass energy and the perturbative expansion is defined by

$$r^{\mathcal{S}}(s) = \sum_{n=0}^{\infty} r_n^{\mathcal{S}}(s) a^{\mathcal{S}n} \qquad (4.11)$$

and $r_0^{\mathcal{S}} = 1$ in all schemes. From this the partial sums of the series can be computed which are defined by
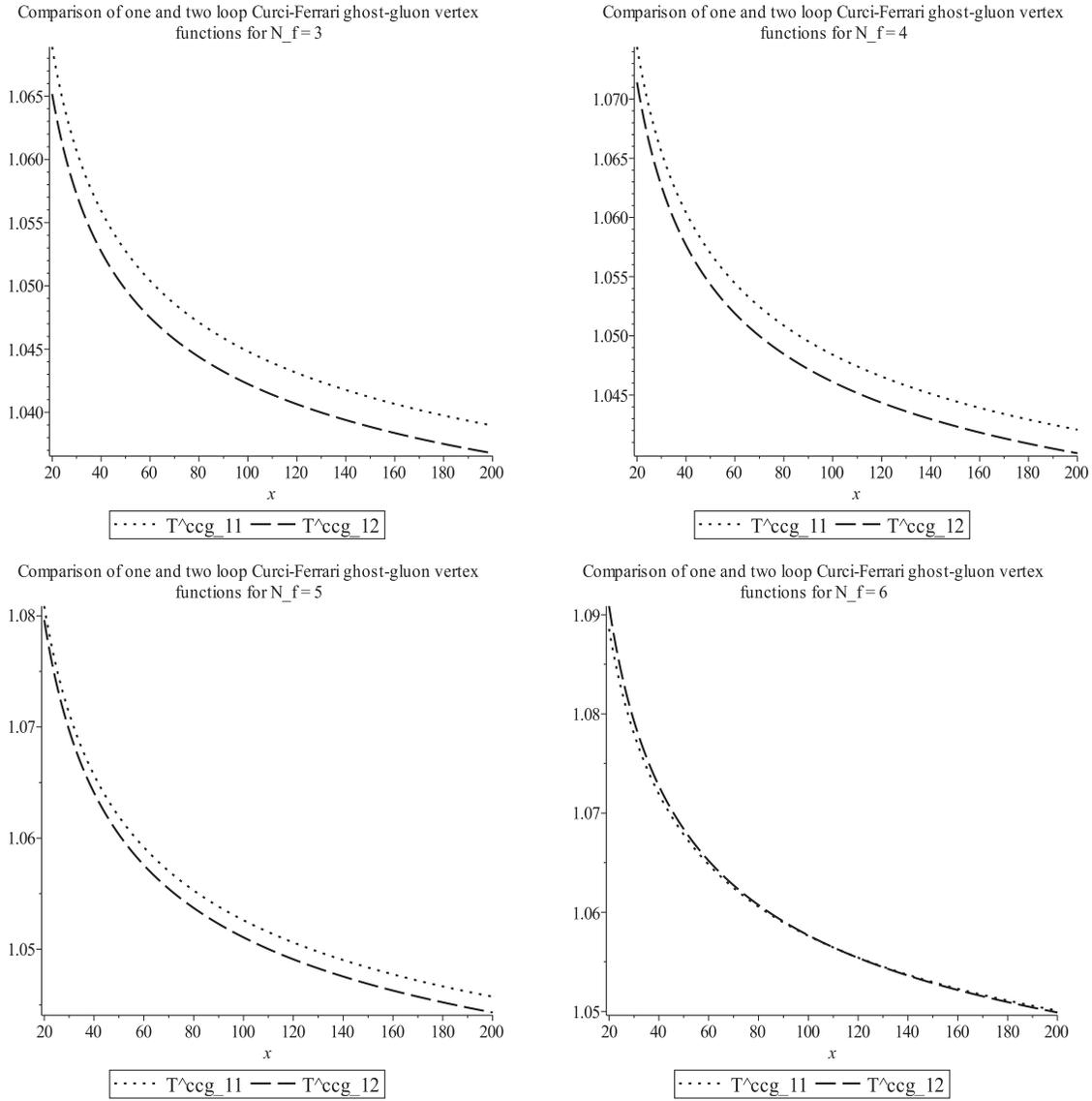
FIG. 3.   Comparison of the $\overline{\text{MS}}$ ghost-gluon vertex function in the Curci-Ferrari gauge for different values of N_f.

$$a_{pq}^{\mathcal{S}}\left(\frac{\mu^2}{\Lambda^{\mathcal{S}2}}\right) = \sum_{n=1}^{p} r_n^{\mathcal{S}}(s)(a_q^{\mathcal{S}}(\mu, \Lambda^{\mathcal{S}}))^n. \qquad (4.12)$$

With these partial sums we have plotted $a_{22}^{\mathcal{S}}(\frac{\mu^2}{\Lambda^{\mathcal{S}2}})$ and $a_{33}^{\mathcal{S}}(\frac{\mu^2}{\Lambda^{\mathcal{S}2}})$ for $N_f = 3$ and 5 and presented representative results in Fig. 4. That we can analyze the two- and three-loop partial sums follows from the fact that we have the coupling constant maps from the MOM schemes to the $\overline{\text{MS}}$ ones at two loops which allows us to construct the R ratio at three loops. This is for the same reason why the three-loop MOM β functions can be constructed in the MAG. In Fig. 4 we have included the $\overline{\text{MS}}$ result to compare with and note that there is close agreement of the MOMq scheme with it. This is not unexpected given that the R ratio is based on a quark operator correlation. As in [80] the

MOMggg and MOMh scheme results lie further away from the $\overline{\text{MS}}$ result due to the nature of the underlying quantity being considered in keeping with the original observations of [38,39]. For larger values of N_f there appears to be a larger discrepancy. However, while this mimics the situation with the canonical linear covariant gauge, if anything the MOM schemes for the MAG lie closer to the $\overline{\text{MS}}$ result than the former gauge. While the broadness of the estimate of the R ratio at a particular center of mass energy scale may appear large on the plot, the range is 5% of a central value if one includes the MOMh scheme. While this may appear to be large, the appropriate point is perhaps that this may be a better way of trying to estimate a theory error in a measurement in contrast to varying the actual running scale between two values chosen in an *ad hoc* manner. What is also evident from these examples is that the specific
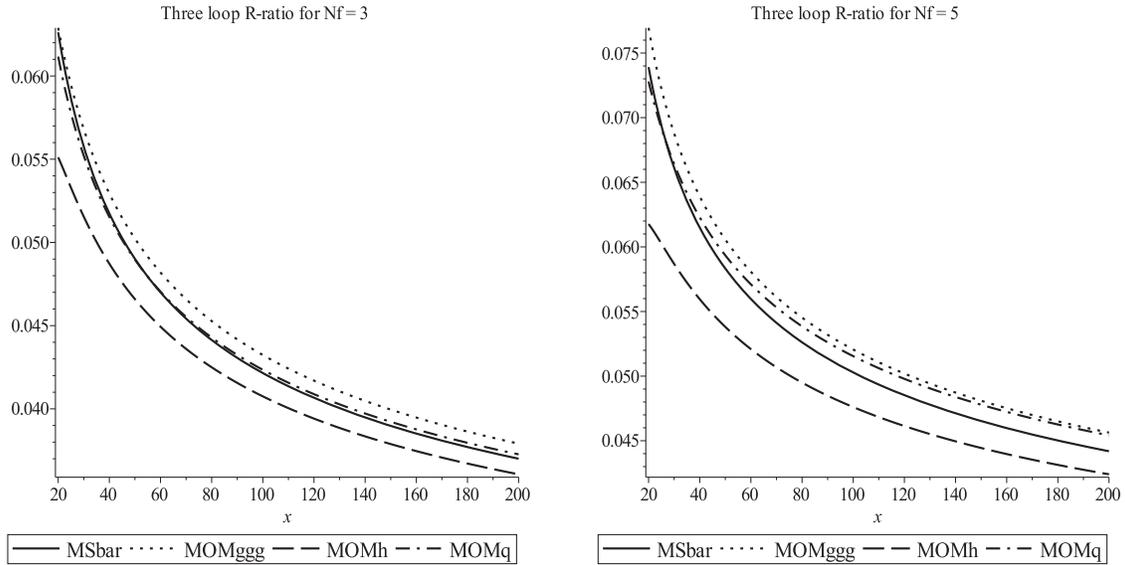
FIG. 4.   Comparison of three-loop R ratio for $N_f = 3$ and 5 in various schemes.

value we have chosen in the MAG here, which is $\alpha = 0$, is in keeping with the $\overline{\text{MS}}$ case which does not depend on the gauge parameter. For instance, in the linear covariant gauge the study of [80] also illustrated that the Landau gauge versions of the R ratio in the corresponding MOM schemes was consistent with $\overline{\text{MS}}$.

While we have considered the effect the various schemes have on a quantity of experimental interest, this was in the chiral limit. While this is an idealized situation, we make brief comments on the complexity of including quark mass effects. First, at high energies quark masses can be neglected as a reasonable approximation. However, for lattice analyses where the matching is performed to merge with the perturbative results such mass effects would be important at the interface region short of the high-energy limit. To estimate the errors on the massless vertex function results by including physical masses is not immediately straightforward in the gauges considered here or in the linear covariant gauge. First, a full quark mass analysis would require all the relevant master integrals at one and two loops with propagators for all the possible quark mass configurations. For two loops these are currently unknown. At one loop, various masters are available, [88,89], and general results are known for the one-loop triple gluon and quark-gluon vertices. For the ghost-gluon vertex the diagrams with a quark propagator do not appear until two loops. Although the general results of [88,89] provide a full analytic structure of the first of these two vertices the nature of the vertex functions even at the symmetric point depend on several Clausen functions whose arguments are ratios of the quark mass and μ^2. However, a symmetric point analysis is too restrictive to quantify quark mass effects. Instead a more appropriate approach would be to compute the corrections to the fully off-shell vertex functions in powers of m_q^2/μ^2 where m_q is a generic quark mass.

Such an analysis is well beyond the scope of the present article.

V. DISCUSSION

The results presented in this article represent the completion of the program of studying QCD fixed in a variety of covariant gauges at two loops at the fully symmetric subtraction point. The one-loop investigation for a linear covariant gauge was initiated several decades ago in [38,39] which was extended to two loops in [70]. In this article we have extended the one-loop MAG and Curci-Ferrari gauge analyses of [37] to the same order as the linear covariant gauge case of [70]. In particular, checks on the MAG results are inextricably entwined with those of the Curci-Ferrari gauge. Although nonlinear gauges are not necessarily the gauges of calculational choice for high-energy analyses, the relation of the MAG to low-energy gluon and quark confinement [3–7,16] suggests that for understanding mechanisms in this regime the MAG will be of analytic importance. While the apparent difference in the ghost-gluon vertices in the MAG and Curci-Ferrari gauges is suggestive of such a picture, that observation is very much still within the perturbative regime. However, having the precision information on the vertex functions given here should ensure that Schwinger-Dyson models, and the assumptions behind the approximations made therein, have independent information to tally with. Ultimately the behavior of Green's functions computed with Schwinger-Dyson techniques have to agree at high energy with perturbation theory. The two-loop results will be useful in this respect. Although ultimately the next order will be of interest, that program requires the determination of the three-loop symmetric point master integrals in the Laporta approach.

[1] D. J. Gross and F. J. Wilczek, Phys. Rev. Lett. **30**, 1343 (1973).

[2] H. D. Politzer, Phys. Rev. Lett. **30**, 1346 (1973).

[3] Y. Nambu, Phys. Rev. D **10**, 4262 (1974).

[4] G. 't Hooft, in *High Energy Physics* (Editorice Compositori, Bologna, 1975).

[5] S. Mandelstam, Phys. Rep. **23**, 245 (1976).

[6] G. 't Hooft, Nucl. Phys. **B190**, 455 (1981).

[7] Z. F. Ezawa and A. Iwazaki, Phys. Rev. D **25**, 2681 (1982).

[8] A. S. Kronfeld, G. Schierholz, and U. J. Wiese, Nucl. Phys. **B293**, 461 (1987).

[9] A. S. Kronfeld, M. L. Laursen, G. Schierholz, and U. J. Wiese, Phys. Lett. B **198**, 516 (1987).

[10] H. Min, T. Lee, and P. Y. Pac, Phys. Rev. D **32**, 440 (1985).

[11] A. R. Fazio, V. E. R. Lemes, M. S. Sarandy, and S. P. Sorella, Phys. Rev. D **64**, 085003 (2001).

[12] K.-I. Kondo and T. Shinohara, Prog. Theor. Phys. **105**, 649 (2001).

[13] T. Shinohara, Mod. Phys. Lett. A **18**, 1403 (2003).

[14] T. Shinohara, T. Imai, and K.-I. Kondo, Int. J. Mod. Phys. A **18**, 5733 (2003).

[15] D. Dudal, J. A. Gracey, V. E. R. Lemes, M. S. Sarandy, R. F. Sobreiro, S. P. Sorella, and H. Verschelde, Phys. Rev. D **70**, 114038 (2004).

[16] N. Sakumichi and H. Suganuma, Phys. Rev. D **90**, 111501 (2014).

[17] A. Cucchieri and T. Mendes, *Proc. Sci.*, LAT2007 (2007) 297.

[18] I. L. Bogolubsky, E. M. Ilgenfritz, M. Müller-Preussker, and A. Sternbeck, *Proc. Sci.*, LAT2007 (2007) 290.

[19] A. Maas, Phys. Rev. D **75**, 116004 (2007).

[20] A. Sternbeck, L. von Smekal, D. B. Leinweber, and A. G. Williams, *Proc. Sci.*, LAT2007 (2007) 304.

[21] I. L. Bogolubsky, E. M. Ilgenfritz, M. Müller-Preussker, and A. Sternbeck, Phys. Lett. B **676**, 69 (2009).

[22] A. Cucchieri and T. Mendes, Phys. Rev. Lett. **100**, 241601 (2008).

[23] A. Cucchieri and T. Mendes, Phys. Rev. D **78**, 094503 (2008).

[24] O. Oliveira and P. J. Silva, Phys. Rev. D **79**, 031501 (2009).

[25] Ph. Boucaud, J. P. Leroy, A. L. Yaounac, J. Micheli, O. Pène, and J. Rodríguez-Quintero, J. High Energy Phys. 06 (2008) 099.

[26] A. C. Aguilar, D. Binosi, and J. Papavassiliou, Phys. Rev. D **78**, 025010 (2008).

[27] C. S. Fischer, A. Maas, and J. M. Pawlowski, Ann. Phys. (Amsterdam) **324**, 2408 (2009).

[28] M. Q. Huber, K. Schwenzer, and R. Alkofer, Eur. Phys. J. C **68**, 581 (2010).

[29] R. Alkofer, M. Q. Huber, V. Mader, and A. Windisch, *Proc. Sci.*, QCD-TNT-II (2011) 003.

[30] V. Mader and R. Alkofer, *Proc. Sci.*, ConfinementX2012 (2012) 063.

[31] T. Suzuki and I. Yotsuyanagi, Phys. Rev. D **42**, 4257 (1990).

[32] S. Hioki, S. Kitahara, S. Kiura, Y. Matsubara, O. Miyamura, S. Ohno, and T. Suzuki, Phys. Lett. B **272**, 326 (1991); **281**, 416 (1992).

[33] A. Mihara, A. Cucchieri, and T. Mendes, *Proc. Sci.*, LATTICE2008 (2008) 243.

[34] T. Mendes, A. Cucchieri, A. Maas, and A. Mihara, arXiv:0809.3741.

[35] S. Gongyo, T. Iritani, and H. Suganuma, Phys. Rev. D **86**, 094018 (2012).

[36] S. Gongyo and H. Suganuma, Phys. Rev. D **87**, 074506 (2013).

[37] J. M. Bell and J. A. Gracey, Phys. Rev. D **88**, 085027 (2013).

[38] W. Celmaster and R. J. Gonsalves, Phys. Rev. Lett. **42**, 1435 (1979).

[39] W. Celmaster and R. J. Gonsalves, Phys. Rev. D **20**, 1420 (1979).

[40] G. Curci and R. Ferrari, Nuovo Cimento Soc. Ital. Fis. **32A**, 151 (1976).

[41] B. S. DeWitt, Phys. Rev. **162**, 1195 (1967).

[42] G. 't Hooft, Acta Univ. Wratislav. **368**, 345 (1976).

[43] B. S. DeWitt, in *Proceedings of Quantum Gravity II*, edited by C. Isham, R. Penrose, and S. Sciama (Oxford University Press, New York, 1980), p. 449.

[44] D. G. Boulware, Phys. Rev. D **23**, 389 (1981).

[45] L. F. Abbott, Nucl. Phys. **B185**, 189 (1981).

[46] D. M. Capper and A. MacLean, Nucl. Phys. **B203**, 413 (1982).

[47] J. A. Gracey, J. High Energy Phys. 04 (2005) 012.

[48] R. Delbourgo, S. Twisk, and G. Thompson, Int. J. Mod. Phys. A **03**, 435 (1988).

[49] J. de Boer, K. Skenderis, P. van Nieuwenhuizen, and A. Waldron, Phys. Lett. B **367**, 175 (1996).

[50] F. Delduc and S. P. Sorella, Phys. Lett. B **231**, 408 (1989).

[51] A. Blasi and N. Maggiore, Mod. Phys. Lett. A **11**, 1665 (1996).

[52] V. Periwal, arXiv:hep-th/9509084.

[53] E. Andriyash and K. Stepanyantz, Moscow Univ. Phys. Bull. **58**, 28 (2003).

[54] G. 't Hooft, Nucl. Phys. **B61**, 455 (1973).

[55] K. G. Chetyrkin and T. Seidensticker, Phys. Lett. B **495**, 74 (2000).

[56] J. A. Gracey, Phys. Rev. D **90**, 025014 (2014).

[57] S. Laporta, Int. J. Mod. Phys. A **15**, 5087 (2000).

[58] J. A. M. Vermaseren, arXiv:math-ph/0010025.

[59] M. Tentyukov and J. A. M. Vermaseren, Comput. Phys. Commun. **181,** 1419 (2010).

[60] P. Nogueira, J. Comput. Phys. **105,** 279 (1993).

[61] C. Studerus, Comput. Phys. Commun. **181,** 1293 (2010).

[62] C. W. Bauer, A. Frink, and R. Kreckel, J. Symb. Comput. **33,** 1 (2002).

[63] A. I. Davydychev, J. Phys. A **25,** 5587 (1992).

[64] N. I. Usyukina and A. I. Davydychev, Phys. At. Nucl. **56,** 1553 (1993).

[65] N. I. Usyukina and A. I. Davydychev, Phys. Lett. B **332,** 159 (1994).

[66] T. G. Birthwright, E. W. N. Glover, and P. Marquard, J. High Energy Phys. 09 (2004) 042.

[67] L. G. Almeida and C. Sturm, Phys. Rev. D **82,** 054017 (2010).

[68] M. Gorbahn and S. Jäger, Phys. Rev. D **82,** 114001 (2010).

[69] See Supplemental Material at http://link.aps.org/supplemental/10.1103/PhysRevD.92.125001 for file with renormalization group functions, coupling constant mappings, conversion functions and amplitudes in analytic form for each gauge.

[70] J. A. Gracey, Phys. Rev. D **84,** 085011 (2011).

[71] J. Ablinger, J. Blümlein, and C. Schneider, J. Math. Phys. (N.Y.) **52,** 102301 (2011).

[72] S. A. Larin and J. A. M. Vermaseren, Phys. Lett. B **303,** 334 (1993).

[73] S. G. Gorishny, S. A. Larin, L. R. Surguladze, and F. K. Tkachov, Comput. Phys. Commun. **55,** 381 (1989).

[74] S. A. Larin, F. V. Tkachov, and J. A. M. Vermaseren, Report No. NIKHEF-H-91-18.

[75] D. R. T. Jones, Nucl. Phys. **B75,** 531 (1974).

[76] W. E. Caswell, Phys. Rev. Lett. **33,** 244 (1974).

[77] J. A. Gracey, Phys. Lett. B **552,** 101 (2003).

[78] O. V. Tarasov, A. A. Vladimirov, and A.Yu. Zharkov, Phys. Lett. **93B,** 429 (1980).

[79] J. Beringer et al. (Particle Data Group), Phys. Rev. D **86,** 010001 (2012).

[80] J. A. Gracey, Phys. Rev. D **90,** 094026 (2014).

[81] K. G. Chetyrkin, A. L. Kataev, and F. V. Tkachov, Phys. Lett. **85B,** 277 (1979).

[82] M. Dine and J. Sapirstein, Phys. Rev. Lett. **43** (1979), 668.

[83] W. Celmaster and R. J. Gonsalves, Phys. Rev. Lett. **44,** 560 (1980).

[84] W. Celmaster and R. J. Gonsalves, Phys. Rev. D **21,** 3112 (1980).

[85] S. G. Gorishnii, A. L. Kataev, and S. A. Larin, Phys. Lett. B **212,** 238 (1988).

[86] S. G. Gorishnii, A. L. Kataev, and S. A. Larin, Phys. Lett. B **259,** 144 (1991).

[87] L. R. Surguladze and M. A. Samuel, Phys. Rev. Lett. **66,** 560 (1991).

[88] A. I. Davydychev, P. Osland, and L. Saks, Phys. Rev. D **63,** 014022 (2000).

[89] A. I. Davydychev, P. Osland, and L. Saks, J. High Energy Phys. 08 (2001) 050.

[90] J. A. M. Vermaseren, Comput. Phys. Commun. **83,** 45 (1994).